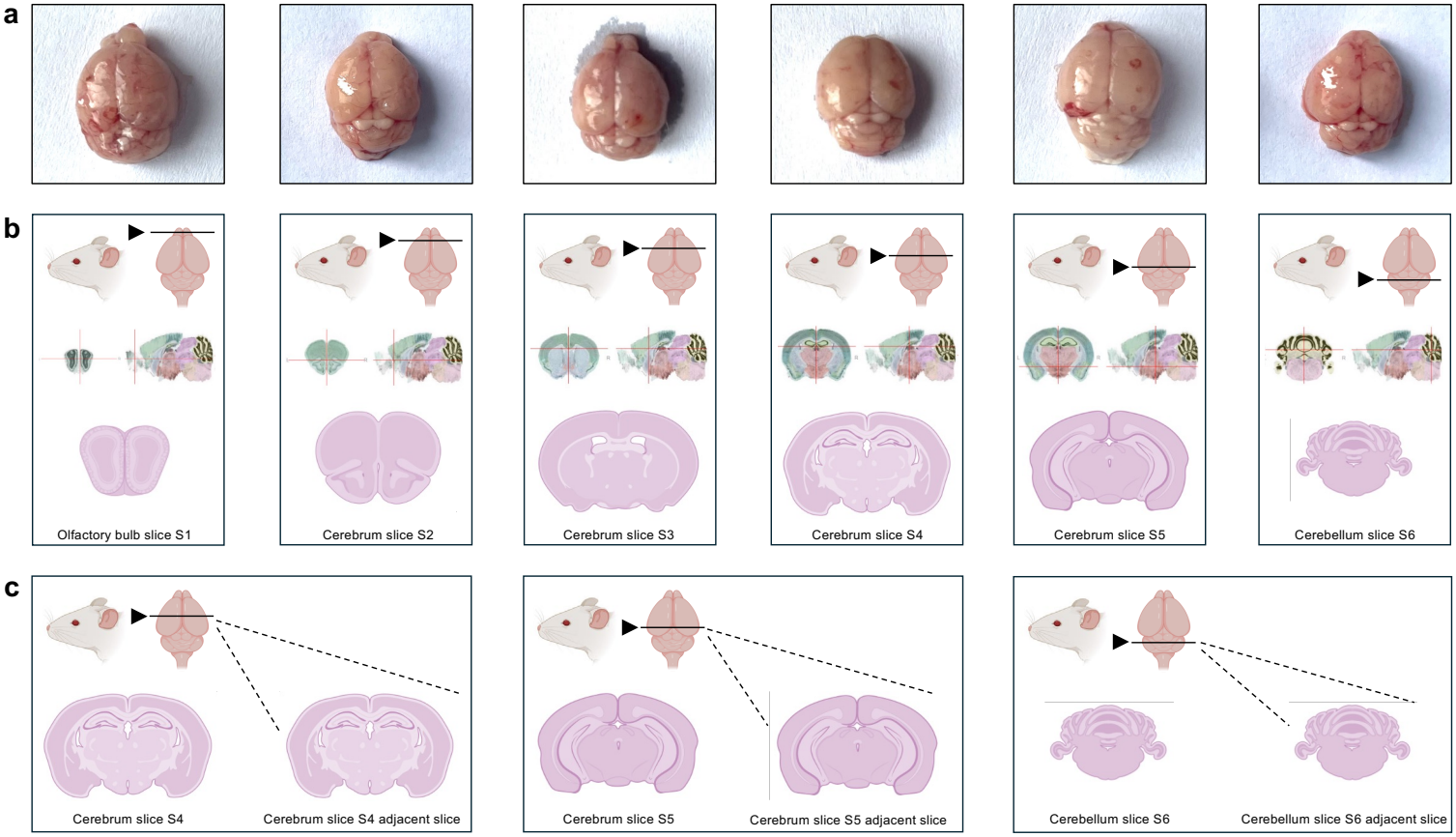
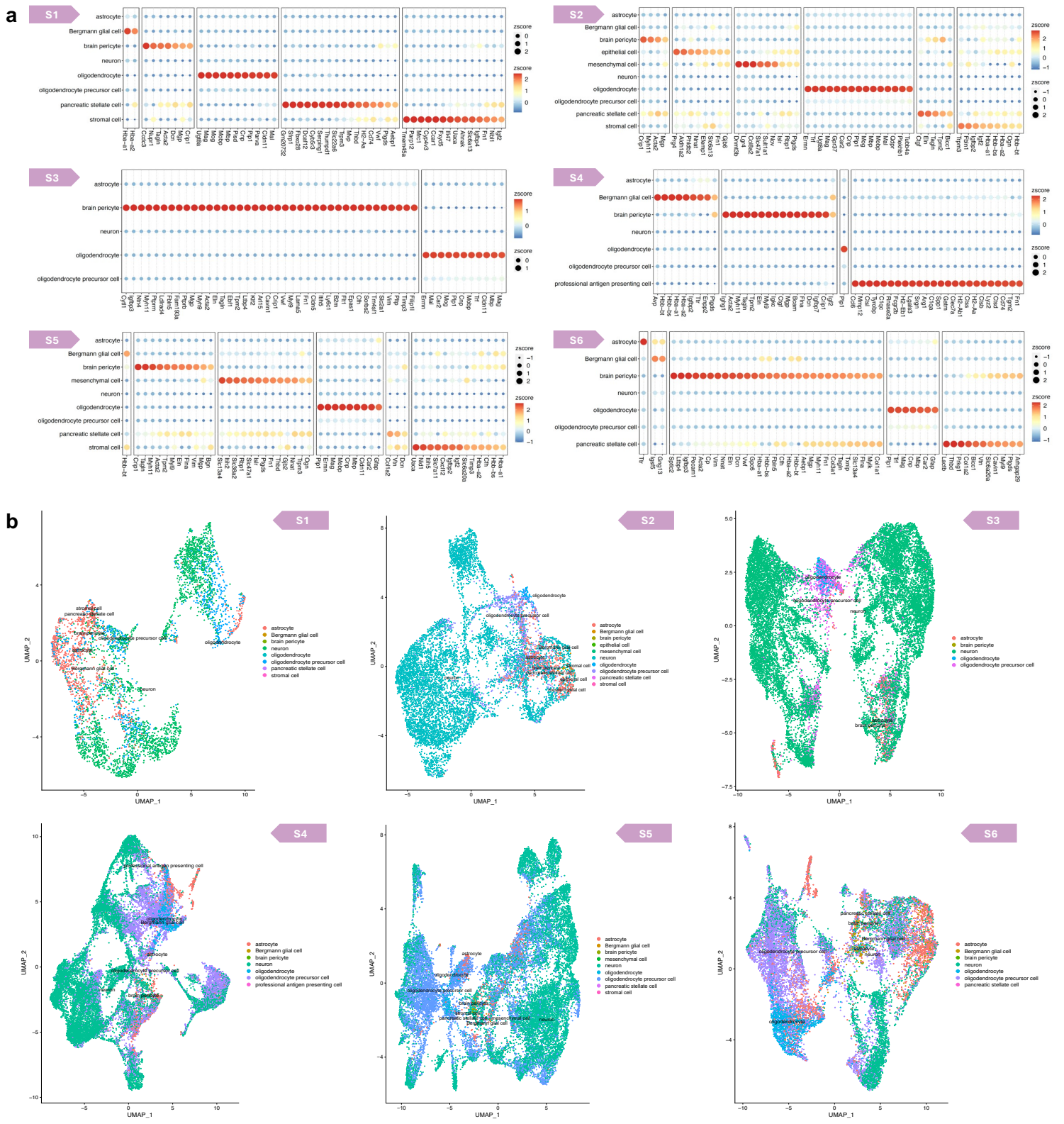
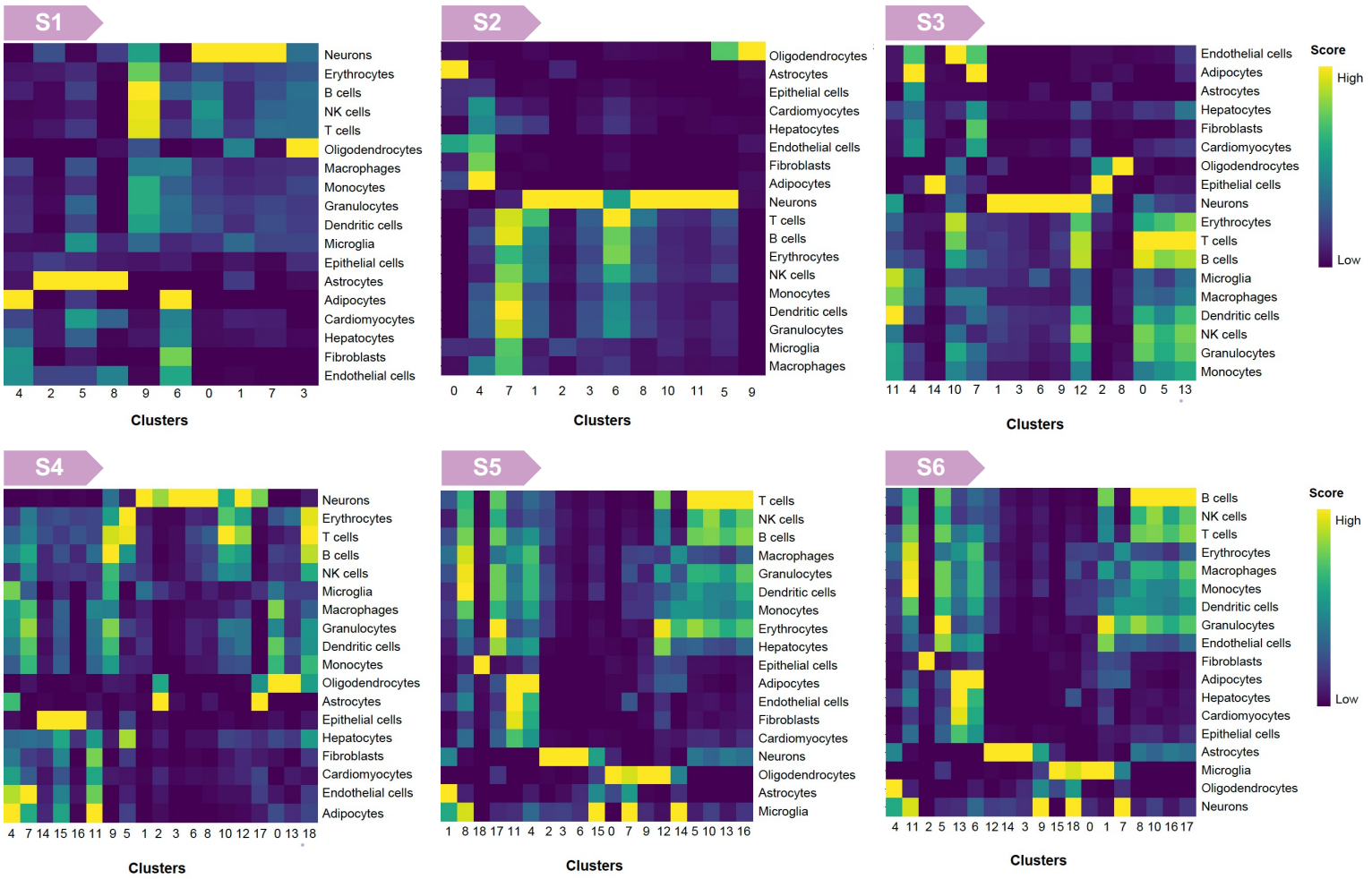


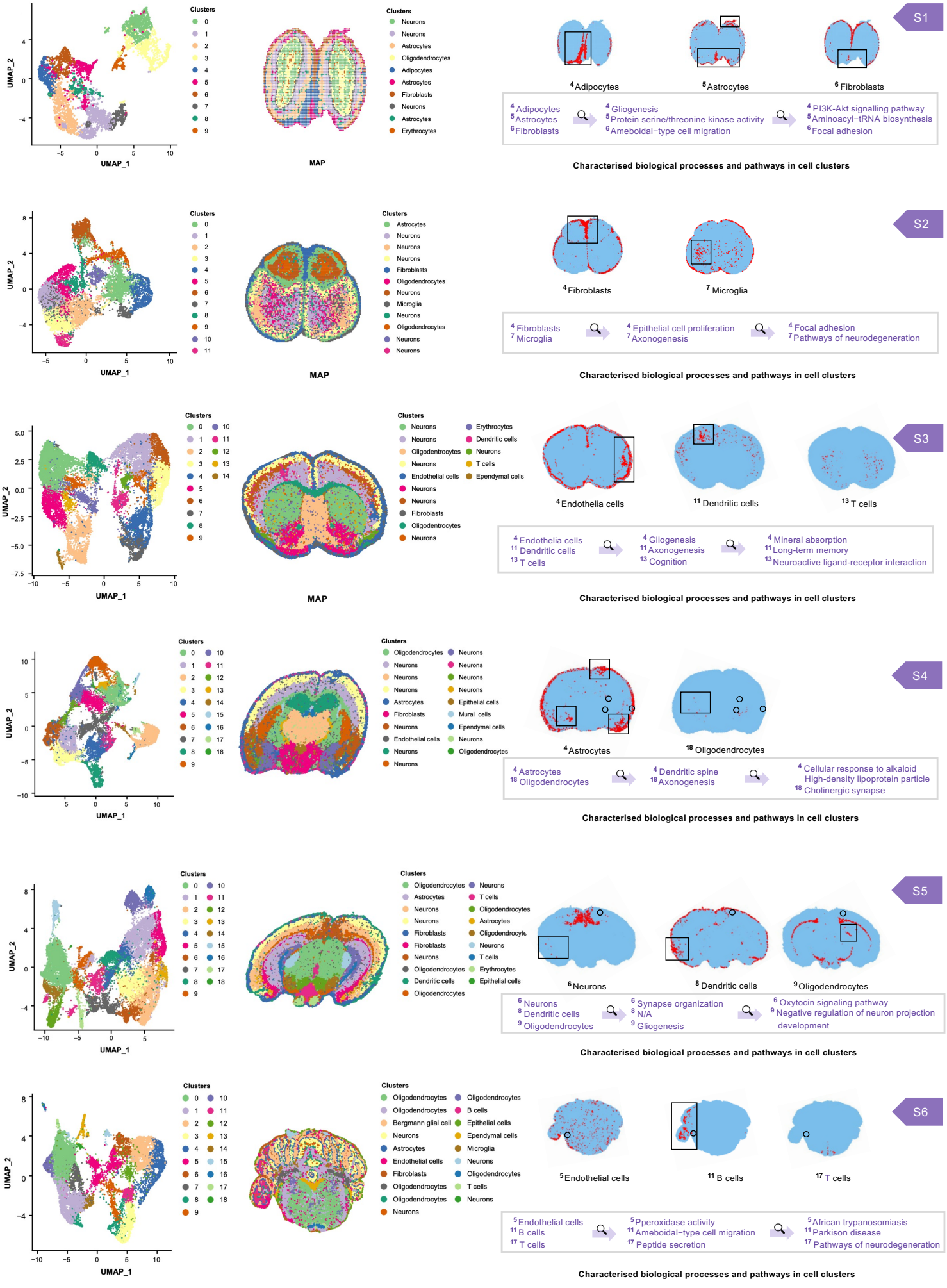
Supplementary Fig. 1 | Murine brain slices subjected to Stereo-seq and single-nucleus RNA sequencing. a Brains collected from mice infected with *Toxocara canis* at 21 days post infection. **b** Schematic diagrams showing the dorsal view of the murine brain and coronal cross-sections of the olfactory bulb (slice S1), cerebrum (slices S2–S5) and cerebellum (slice S6) collected from *Toxocara canis*-infected BALB/c mice. Lesions and migrating larvae are indicated by red and blue dots, respectively. **c** Schematic diagrams showing coronal brain slices adjacent to cerebrum slices S4 and S5, and cerebellum slice S6, containing migrating *T. canis* larvae. Created in BioRender. Zou, M. (2026) https://BioRender.com/n5n4bbj.



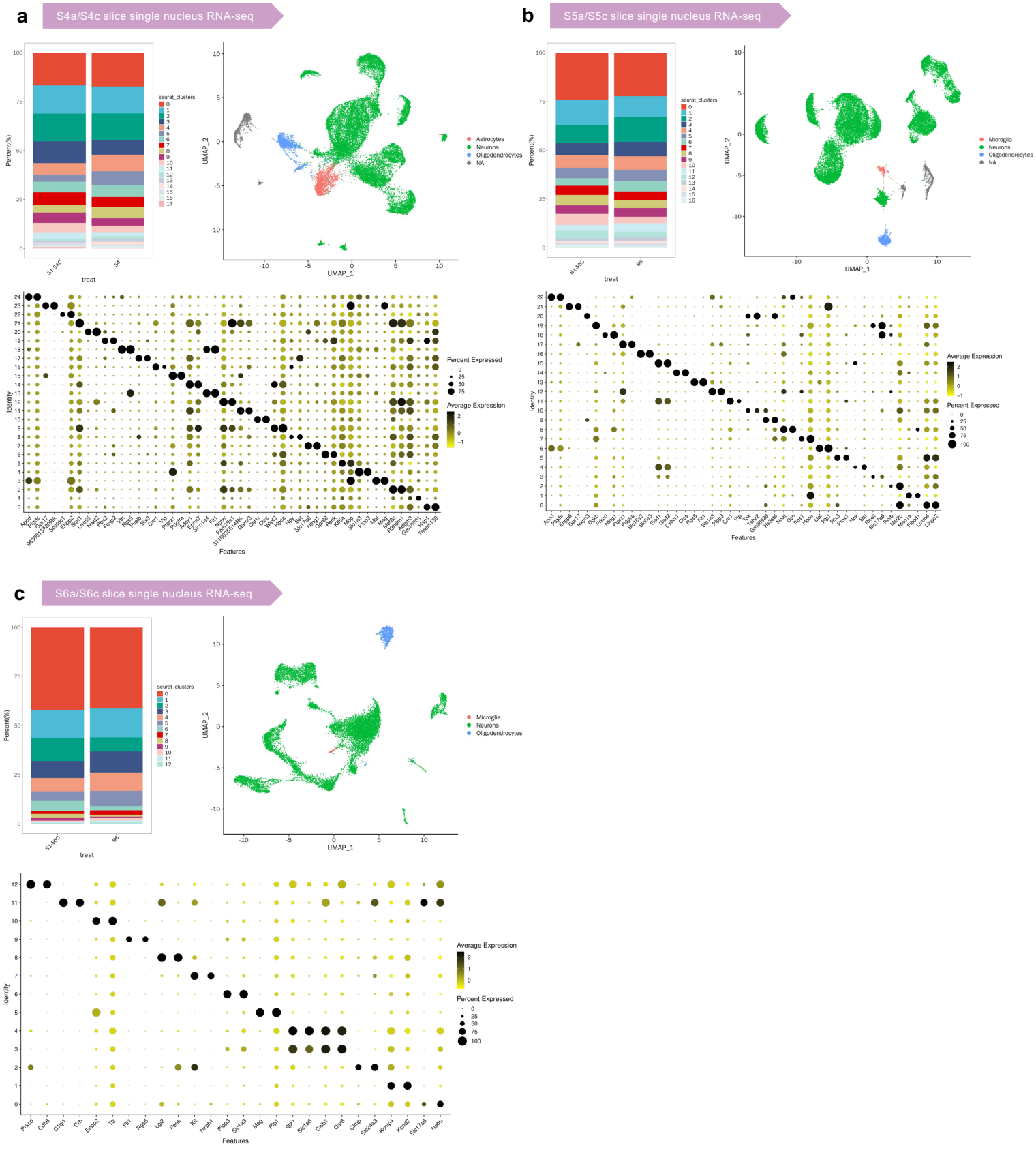
Supplementary Fig. 2 | Cell clustering, marker selection and annotation based on Stereo-seq data. a Heatmap of selected gene transcripts defining cell clusters in different slices of the murine olfactory bulb (S1), cerebrum (S2–S5) and cerebellum (S6) – using public reference data for mammalian cells. **b** SciBet-scale UMAP plots showing annotation of murine cell populations in these different slices. In S1, astrocytes, Bergmann glial cells, brain pericytes, neurons, oligodendrocytes, oligodendrocyte precursor cells (OPCs), stromal cells and a pancreatic stellate-like cluster were identified. In S2, astrocytes, Bergmann glial cells, brain pericytes, epithelial cells, mesenchymal cells, neurons, oligodendrocytes, OPCs, stromal cells and a pancreatic stellate-like cluster were detected. In S3, astrocytes, brain pericytes, neurons, oligodendrocytes and OPCs were identified. In S4, astrocytes, Bergmann glial cells, brain pericytes, neurons, oligodendrocytes, OPCs and professional antigen-presenting cells were annotated. In S5, astrocytes, Bergmann glial cells, brain pericytes, mesenchymal cells, neurons, oligodendrocytes, OPCs, stromal cells and a pancreatic stellate-like cluster were found. In S6, astrocytes, Bergmann glial cells, brain pericytes, neurons, oligodendrocytes, OPCs and a pancreatic stellate-like cluster were identified.



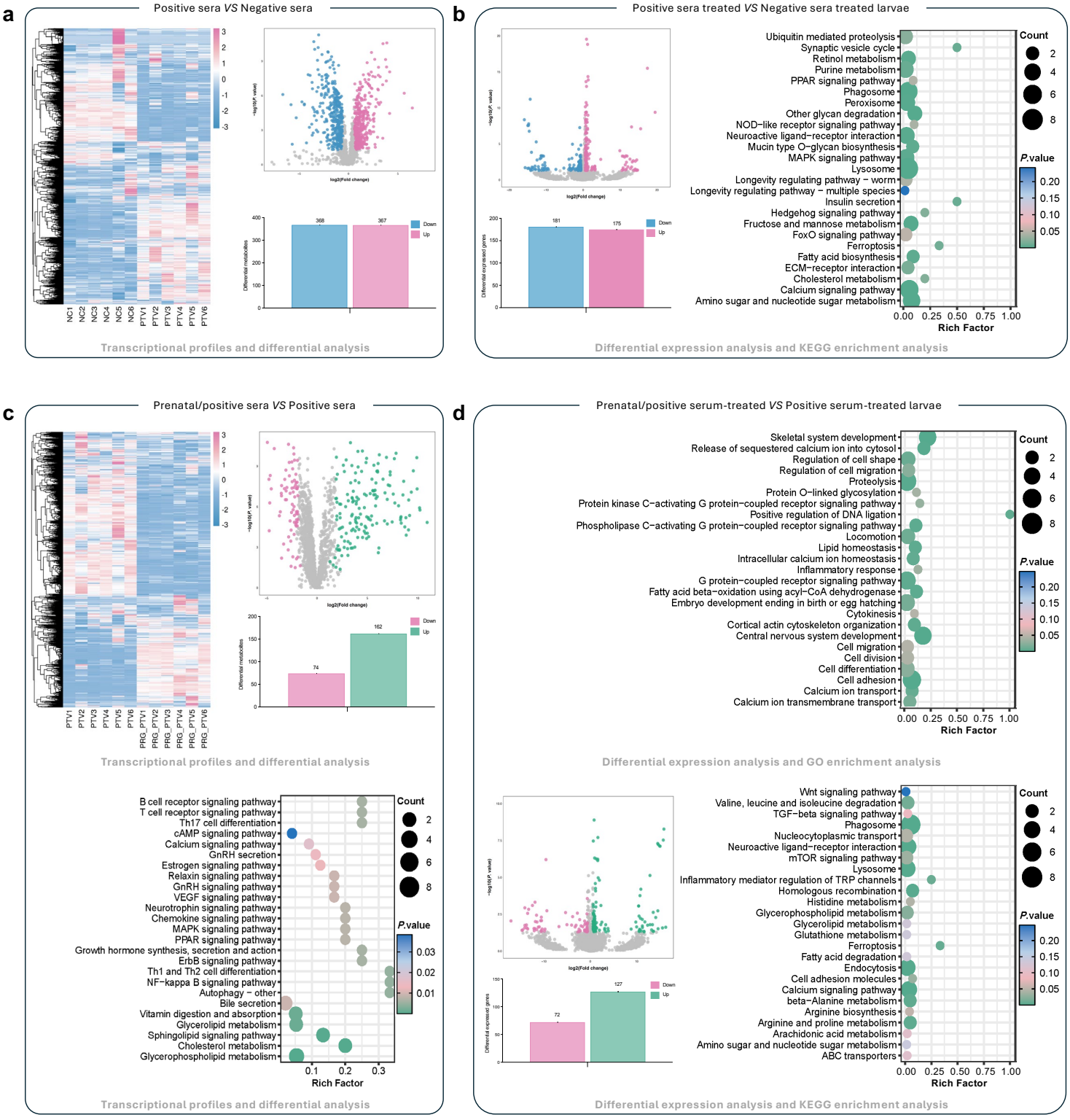
Supplementary Fig. 3 | Marker selection and annotation based on Stereo-seq data. Violin plots showing the transcription levels of marker genes identified for neurons, erythrocytes, B cells, natural killer (NK) cells, T cells, oligodendrocytes, macrophages, monocytes, granulocytes, dendritic cells, microglia, epithelial cells, astrocytes, adipocytes, cardiomyocytes, hepatocytes, fibroblasts and endothelial cells across the murine olfactory bulb (slice S1), cerebrum (slices S2–S5) and cerebellum (slice S6).



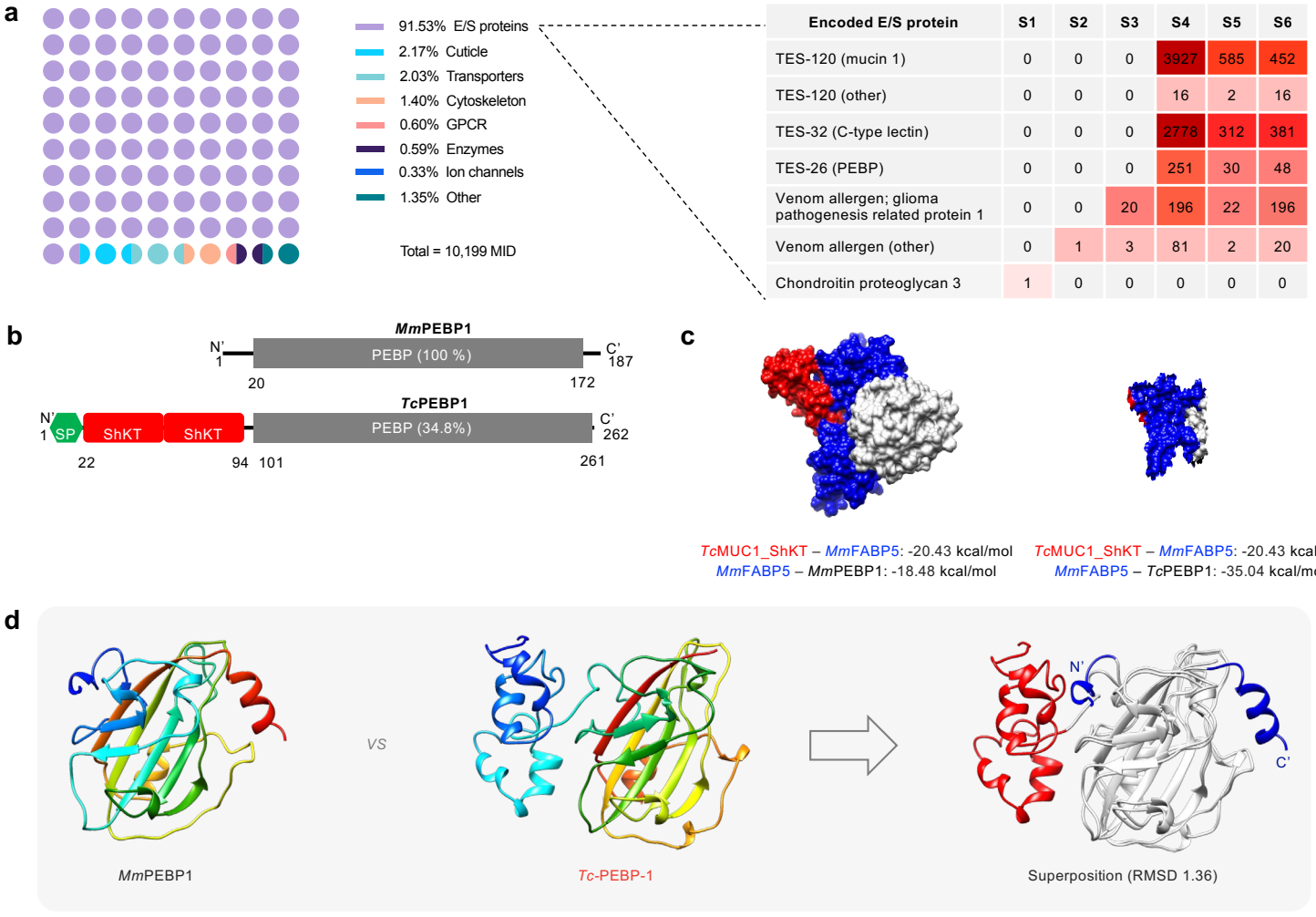
Supplementary Fig. 4 | Spatial cell atlas of *Toxocara canis*-invaded brain sections. Annotation and spatial mapping of cell clusters in the olfactory bulb (S1), cerebrum (S2–S5) and cerebellum (S6) slices. Unsymmetrical distributions of neuronal and immune cell populations are highlighted in black boxes. Areas of migrating larvae are indicated in black circles. Associated Gene Ontology biological processes (e.g., ameboid-type migration, peroxidase activity, gliogenesis, cognition) and pathways (e.g., PI3K–Akt signalling, neurodegeneration, long-term memory) are summarised.



Supplementary Fig. 5 | Single-nucleus RNA sequencing, cell clustering, and annotation of infected and uninfected brains. Cell clustering, marker gene identification and annotation of murine cerebrum and cerebellum slices are shown. Annotated cell clusters include astrocytes, epithelial cells, neurons and oligodendrocytes in the slices adjacent to slices S4/5/6 (S4/5/6a) and controls (S4/5/6c).



Supplementary Fig. 6 | Influence of murine immune defence on *Toxocara canis* larvae *in vitro*. **a** Differential lipid metabolite analysis between positive (PTV) sera (n = 6) and negative control (NC) sera (n = 6) from *T. canis*-infected mice. Metabolites with significantly higher (n = 367) or lower (n = 368) abundance (fold change > 1.5, p < 0.05) in PTV sera compared to NC sera are shown in volcano and bar plots. **b** Differential transcriptomic analysis of *T. canis* larvae treated with PTV or NC sera *in vitro*. Genes with significantly altered transcript levels (fold change > 1.5, p < 0.05) are shown in a volcano plot. Kyoto Encyclopedia of Genes and Genomes (KEGG) pathway enrichment analysis is presented in a dot plot, indicating gene number, rich factor and P value. **c** Differential lipid metabolite analysis between prenatal and positive (PRG_PTV) sera (n = 6) and PTV sera (n = 6). Metabolites with significantly higher (n = 162) or lower (n = 74) abundance (fold change > 1.5, p < 0.05) are shown in volcano and bar plots. KEGG pathway enrichment of differentially abundant metabolites is shown in a dot plot. **d** Differential transcriptomic analysis of *T. canis* larvae treated with PRG_PTV or PTV sera. Genes with significantly altered transcript levels (fold change > 1.5, p < 0.05) are shown in a volcano plot. Gene Ontology (GO) and KEGG pathway enrichment of differentially transcribed genes is shown in dot plots, with gene number, rich factor and P value indicated.



Encoded E/S protein	S1	S2	S3	S4	S5	S6
TES-120 (mucin 1)	0	0	0	3927	585	452
TES-120 (other)	0	0	0	16	2	16
TES-32 (C-type lectin)	0	0	0	2778	312	381
TES-26 (PEBP)	0	0	0	251	30	48
Venom allergen; glioma pathogenesis related protein 1	0	0	20	196	22	196
Venom allergen (other)	0	1	3	81	2	20
Chondroitin proteoglycan 3	1	0	0	0	0	0

Supplementary Fig. 7 | Immune evasion and modulation by migrating *Toxocara canis* larvae. a Proportion of protein families encoded by *T. canis* genes in murine brain slices based on Stereo-seq data. Excretory/secretory (ES) protein-coding genes constitute 91.53% of total detected genes. Expression levels of mucins (TES-120), C-type lectins (TES-32), phosphatidylethanolamine-binding proteins (TES-26), venom allergen-like proteins and chondroitin proteoglycans are shown in a heatmap based on molecular identity (MID) counts. **b** Domain architecture and structural comparisons between *T. canis* PEBP1 and murine PEBP1. **c** Structural comparison of protein complexes comprising *T. canis* MUC1 (*Tc*-MUC-1) ShKT domains, murine FABP5 (*Mm*FABP5) and PEBP1 (*Mm*PEBP1), versus *Tc*-MUC-1 ShKT domains, *T. canis* PEBP1 (*Tc*-PEBP-1) and *Mm*FABP5. *Tc*-PEBP-1 shows stronger predicted binding to *Mm*FABP5 (-35.04 kcal/mol) than its murine orthologue (-18.48 kcal/mol).